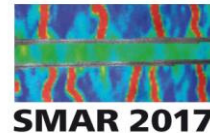University of
Strathclyde
Glasgow

McAlorum, J. and Mckeeman, I. and Perry, M. and Clayburn, L. and Niewczas, P. (2017) Predicting freeze-thaw damage using tipping point analysis of strain data. In: SMAR2017, 2017-09-13 - 2017-09-15, ETH Zurich. ,

This version is available at https://strathprints.strath.ac.uk/61876/

Predicting Freeze-Thaw Damage using Tipping Point Analysis of Strain Data

J. McAlorum[1], I. McKeeman[1], M. Perry[2], L. Clayburn[1], and P. Niewczas[1]

[1] Electronic and Electrical Engineering, University of Strathclyde, Glasgow, UK
[2] Civil and Environmental Engineering, University of Strathclyde, Glasgow, UK

ABSTRACT: This paper demonstrates how Tipping Point Analysis can be used to predict the onset of structural strain, induced by ice formation. In civil structures, water-ice transitions present many potential issues that can lead to structural damage or plant shutdowns. Examples include freeze-thaw damage in concrete and masonry, and ice build-up on moving parts such as wind turbine blades. Early indication of ice formation could prevent irreparable damage if this information could be used to actuate de-icing procedures. The transition considered in this work is the strain induced in a polypropylene container by the volume change of water as it freezes, measured using surface-mounted fibre-optic strain sensors. This first order phase transition can be detected early on using degenerate fingerprinting, which identifies "slowing down" of the noise prior to the critical point of the transition.

Water was supercooled which, at freezing, causes a rapid increase in temperature, presenting an identifiable specific transition point for reference. The analysis was able to consistently predict freezing around 5-10 minutes prior to the transition. A linear relationship was found between mass calculated from the calorimetric equation and mass from experimental measurements. Strain could not be estimated from this mass, since the random process of freezing in an open top container causes an irregular distribution of force. These tests will allow the method and the model to be continually developed towards a more practical application.

1 INTRODUCTION

Structural Health Monitoring (SHM) can be defined as continuous assessment of normal operating conditions and/or any existing damage of the structure. SHM is used in many industries such as civil Ko et al (2003), aeronautical Nicolas et al (2016), oil and gas Inaudi et al (2006). The most desired and currently implemented SHM systems involve civil, transport, marine, oil and gas, and power network infrastructure, with many employing fibre Bragg gratings (FBGs) for health monitoring Chan et al (2006) Lima et al (2008) Bai et al (2016). FBGs present many advantages over conventional electronic strain sensors, such as immunity to electromagnetic interference, multiplexing ability and small size Kashyap et al 2010. Robust, long-life designs are also achievable Niewczas et al (2011).

The objective of this work is to develop a system capable of predicting and alerting of the freezing transition of water – to be used to initiate de-icing procedures to prevent ice formation.

1.1   Potential Applications

The system described has potential applications in many fields where ice formation is undesirable: examples include aeronautical, civil and electrical power engineering; and even biochemistry and culinary science. In the context of civil engineering, for example, FBGs have already shown promise in monitoring reinforced concrete structures. A common degrader of concrete in colder climates is freeze-thaw: damage is accrued with the introduction of water, which expands upon freezing causing cyclic stress and damage over multiple freeze-thaw cycles Li et al (2016). The forms of damage caused by freeze-thaw range from exterior damage to the outer layer of concrete known as scaling or pop-outs, to internal damage and crack initiation or expansion Harrison et al (2001). Eventually, these cracks can provide a pathway for corroding agents to attack the underlying steel reinforcement, reducing the structure's tensile strength. Concrete freeze-thaw damage is a common and ongoing concern for infrastructure managers, since the effects only become visibly apparent after significant degradation. The method we propose here could be used to inform manual maintenance or could be used in conjunction with a simple, automatically triggered heating element to prevent ice formation.

An ice detection system for wind turbine blades is another example where the system we have demonstrated would be valuable. Methods currently employed include detection via changes in low frequency vibration signals caused by imbalance due to weight of ice, or by anemometry slowing compared to wind speeds due to ice buildup. In both cases, significant ice formation is required for detection. Usually, visual-inspection follows detection to ensure existence of ice. Switching the turbine off and on is a simple way to forcibly remove the ice, some turbines have heated blades that remove ice. Our method would improve the efficiency of both of these systems as they would only need to be used when required.

1.2   Competing technologies

There are many proposed ice detector systems, including those currently implemented, reviewed by Cattin et al (2015). They measure factors affected by ice such as: humidity changes, speed variation of rotating objects (e.g. anemometers), vibration fluctuations on a probe, refraction or blocking of light, and natural frequency alterations. The common issues these sensors face include inefficient ice detection due to indirect measurements of key measurands, and that the sensors require a significant amount of ice to form before indication is possible.

1.3   Background

1.3.1   FBG Functionality

An FBG sensor is formed by exposing an optical fibre to an Ultra Violet light of modulating intensity to create a periodic alteration of the refractive index. When broadband light is projected through the FBG, it reflects a range of wavelengths of the incident light with a distinctive peak at the Bragg wavelength, λ_B. The peak wavelength is determined during production of the FBG and is a function of grating period, Δ, and effective refractive index, η_e, of the fibre Rao et al (1996).

$$\lambda_b = 2\eta_e\Delta \qquad\qquad (1)$$

Both variables in Equation 1 are mainly affected by strain and temperature Hill et al (1997). Equation 2 shows the effects on the reflected wavelength of a bonded FBG due to a change in temperature, ΔT, and strain, ϵ. Constants, k_t and k_ϵ, are the temperature coefficient and strain sensitivity after bonding, respectively. A separate unbonded FBG, which does not measure strain (i.e. $k_\epsilon = 0$) is usually added for temperature compensation.

$$\frac{\Delta \lambda_\epsilon}{\lambda_\epsilon} = k_t \Delta T + k_\epsilon \epsilon \qquad (2)$$

1.3.2 Ice Formation – First Order Phase Transitions

In a number of physical systems, approaching a critical point causes "slowing down" of the noise in some key measurands. This occurs due to the energy levels between two states shifting as the system approaches a transition (see Figure 1), causing the gradient of walls between potential minima to decrease. Figure 1 illustrates the molecular process of transition from a lower to a higher volume state, such as is the case for the first order water-ice phase transition. Minima containing molecule A at temperature T1 represents liquid phase and at T3 the solid phase. For a constant pressure, when T1 decreases to T3 nucleation occurs, ice forms and volume is increased. At T2 the energy required to transition has decreased, which decreases the oscillation (noise) frequency indicated by the dashed double arrow curve.
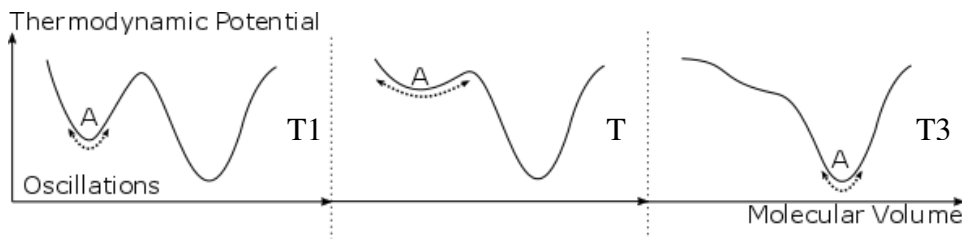

Figure 1. First order phase transition. Molecule A resides in the lower volume state initially. Energy required to transition to increased volume state decreases with temperature (T1 > T2 > T3), causing "slowing" of noise oscillations before transition.

1.3.3 Tipping Point Analysis

It has been demonstrated previously that state transitions in time series data can be identified early using Tipping Point Analysis (TPA) Perry et al (2015) Livina et al (2015). Many different approaches are possible when attempting this as the data can demonstrate many interesting aspects such as memory, variability and "flickering" Dakos et al (2012). For this work, the memory analysis method called "degenerate fingerprinting" was deemed most suitable due to the first order phase transition behavior. The water-ice transition is indicated by an increase in volume. This increase in volume can be indirectly detected via the strain increase it induces in a surrounding solid medium. In an applied context, this could be the walls of the crack, but in our laboratory experiment, it is the walls of an enclosure. Equation 3 shows that total strain measured in the walls of the enclosure, $\epsilon_T(t)$, is a sum of static (or relatively slowly changing) strain in component, $\epsilon_0(t)$ and Gaussian noise $\epsilon_n(t)$.

$$\epsilon_T(t) = \epsilon_0(t) + \epsilon_n(t) \qquad (3)$$

As discussed in section 1.3.2, the oscillation of the system about the minima creates the noise, $\epsilon_n(t)$, and this noise "slows down" when the system approaches a critical transition. In most cases, the noise will be filtered out to ensure a more accurate measurement of component strain. However, in this case, the noise is utilized to provide an indicator of future events of the system. Degenerate fingerprinting uses lag-1 auto-correlation on a sliding window of extracted noise data to detect trends in the noise that are symptomatic of slowing down behavior. Assuming a window of noise data, $Z_{t=1:N}$, the auto-correlation function, ρ_k, can be calculated using Equation 4.

$$\rho_k = \frac{\sum_{t=1}^{N}(Z_t - \mu)(Z_{t+1} - \mu)}{\sum_{t=1}^{N}(Z_t - \mu)^2} \tag{4}$$

Where μ is the expected value of Z_t and N is the length of the window. Should the transition be detected, ρ_k should begin to rise to a value of 1, as slow noise shows a strong auto-correlation.

1.3.4 Water-Ice Transition Model

Gholaminejad et al (2013) produced an extensive study into the process of supercooling. At the point of forced nucleation, the water temperature would instantly rise to 0°C in some cases from temperatures as low as -5°C. In contrast, the process was not forced in this work, but occurred randomly during experimentation. This temperature rise provided a reference point of ice formation to be used during analysis. Any increase in volume (and hence strain) due to freezing should coincide with the onset of temperature increase, at which point only a fraction of the water mass has transitioned to ice mass, m_{ice}. Ice can form initially in multiple ways in an open top container: top layer first (usually in larger bodies of water), on all walls first or both simultaneously. Since the thermal conductivity of polypropylene (0.2 W/mK) is greater than that of air (0.024 W/mK), ice should form first on the container walls.

The strain measured on the wall of the container is caused by the rapid expansion of ice. Unfortunately, due to unknown factors such as number of impurities, exact amount of ice formed and position of nucleation center the strain is difficult to accurately predict. Qualitatively, we can assume that more ice forming causes higher strain. Estimation of ice mass formed by supercooled water freezing can be made by equating the heat energy provided by the exothermic water-ice transition to the reduction in internal energy going from supercooled water to ice Bochnicek et al (2014) (Equation 5).

$$m_w c \Delta T_S = m_I l_f \tag{5}$$

Where m_w is the mass of water, c is the specific heat capacity of liquid water (4181 $J/kg°C$), ΔT_S is the increase in temperature at freezing point, l_f is the latent heat of fusion of ice (333550 J/kg) and m_I is the estimated mass of ice. To test this hypothesis, m_{ice} and ΔT_S were measured for multiple freezing cycles and compared to estimated mass m_I (Table 1).

Table 1. Calculated mass compared to measured mass of freezing cycles of tap water.

ΔT (°C)	Ice mass, m_{ice}, (g)	Calculated mass, m_I, (g)	$\dfrac{m_{ice}}{m_I}$
1.2	27.64	7.56	3.66
1.4	31.56	8.82	3.58
1.8	34.32	11.34	3.03
2.9	57.10	18.27	3.13
4.0	99.50	25.20	3.95
5.4	119.72	34.01	3.52

These tests show that the mass of ice that forms, m_{ice}, is on average 3.48 times greater than m_I, calculated using Equation 5. The equation does not take into account the type of water used. This may be an issue since the rate that ice forms depends on the number of nucleation sites (including impurities) in the water, shown in Equation 6.

$$R = K_p \exp(-\frac{\Delta G}{k_B T}) \tag{6}$$

Where K_p is a constant which contains the number of nucleation sites and the rate at which molecules attach to the nucleus. ΔG is the change in Gibbs free energy of the nucleus at transition, k_B is the Boltzmann constant and T is the temperature. Work by Stott et al (2008) has shown that the rate of ice formation in purified water varies from $0.0006 - 0.023 \ ms^{-1}$. Purified water has around 10-50 parts per million (PPM) of total dissolved solids (representing number of nucleation sites in K_p), whereas still tap water is known to have around 300-600 PPM. This difference may cause a variation in the rate of ice formation, which may change the structure of the ice crystal itself, which may in turn have an impact on the mass of ice formed.

2 METHODOLOGY
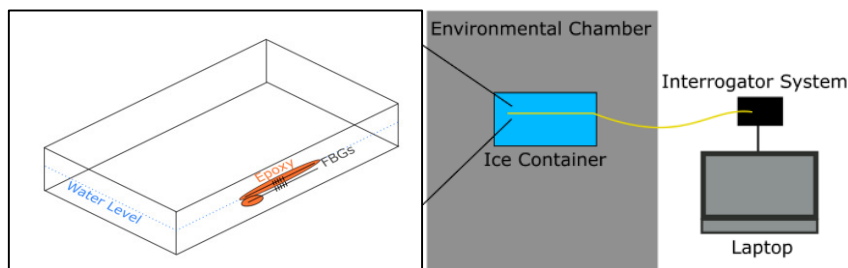
2.1 Experimental Setup

Figure 2. Experimental set up.

To demonstrate the method of predicting ice formation as described in Section 1.3.3, a polypropylene container (low Young's modulus) was filled with 0.5 l of regular tap water and instrumented with an FBG measuring strain and an FBG measuring temperature to compensate for thermal effects (Figure 2). Container was placed within an environmental chamber to ensure consistent freezing cycles and sensors were connected to an FBG interrogator with sampling frequency of 50 Hz with a laptop interface (Figure 2). The strain FBG was fully epoxied along the water level, whereas the temperature FBG was epoxied on one side to ensure thermal contact only. Finally, thermal grease was applied over both to ensure equal heat transfer for both sensors. A total of seven freezing cycles were run under the same conditions, with the environmental chamber programmed to begin at 25°C and cool to -14°C for a period of around 5 hours, after which the ice was fully melted before repeating the cycle.

2.2 Results

To perform TPA, the noise from the strain FBG was first extracted by using a moving average to remove trend, acquiring the noise signal only. Lag-1 autocorrelation (Equation 4) was performed on the noise signal over a sliding, self-intersecting window as described in section 1.3.3. The analysis was performed over the entire freezing cycle. The final result is an autocorrelation function (ACF) indicator for each freezing cycle. The window size over which ACF was calculated was adjusted to provide the most significant indication in each cycle. Window size is dependent on a few factors, some of which are defined initially and remain constant such as the sampling rate or length of event. System's dynamics however, can vary for each cycle, requiring adjustment of the window size. Currently, the choice of window size can be informed through sensitivity analysis and the experimenter's understanding the time dependence of the system's

dynamics. However, in future work, we aim to develop an algorithm to automatically determine window size.

For a successful prediction, the ACF indicator should display a trend towards 1 prior to the transition Livina et al (2007), which has been time-stamped as the point of freezing. In a single experiment, seven freezing cycles were run on the same body of water. Figure 3 portrays four examples of cycles where an early indication was significantly apparent and provided an alert. ACF window size for cycles one, two, and seven was 50,000 data points (16 minutes 40 seconds), and for cycle four it was 10,000 data points (3 minutes 20 seconds).
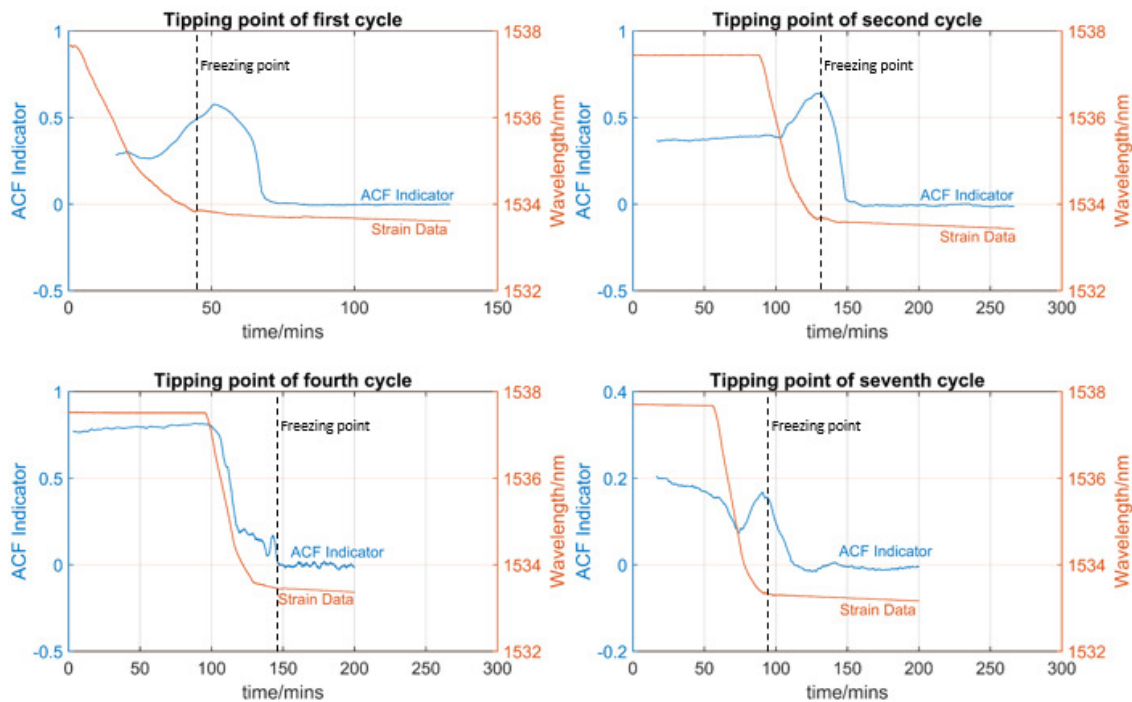

Figure 3. Tipping point results of four freezing cycles, all of which provided early detection prior to ice formation.

In the cases of the first, second and seventh freeze, the indicators trend to 1 is clearly apparent and would be easy to identify with a simple automatic detection system. In the fourth freeze, there is a noticeable increase which could be identified by eye, but would depend on the sensitivity of the detection system. These results all provided an alert around 5-10 minutes prior to the freezing point. The further three cycles provided insufficient rise in indicator to provide an alert – they did not provide any false positives either. This means the ACF calculation did not find sufficient evidence to provide a rise. To understand why, we can first look at the temperature compensated strain values. Table 2 provides the strain values, extracted in each cycle using the temperature FBG for compensation in Equation 2. Using Equation 5 we can calculate the ice mass at freezing point, then provide an estimate for the real mass formed in the experiment (3.48 times greater than m_I).

Table 2. Strain on container wall in each cycle – bold text indicates successful predictions (cycles 1, 2, 4 and 7).

Cycle #	Strain in FBG $\epsilon_0(t)$ $\mu\epsilon$	Temperature increase ΔT_S $°C$	Calculated mass (m_I) g	Estimated mass (m_{ice}) g
1	**28.687**	**1.760**	**11.086**	**38.579**
2	**27.386**	**1.735**	**10.929**	**38.033**
3	32.604	1.443	9.090	31.633
4	**13.043**	**1.915**	**12.060**	**41.969**
5	13.042	1.750	11.020	38.350
6	6.521	1.875	11.811	41.102
7	**22.826**	**1.361**	**8.398**	**29.225**

From this set of data and experimental set up, we can conclude that the measured strain is uncorrelated with the ice mass that forms at freezing. For example, cycle 4 had the largest temperature rise, thus largest estimated mass, but only the 5th highest strain. The reasons for this: ice does not form on the single instrumented wall alone and may not from equally on all walls, behavior of ice expanding is influenced by the open air and surrounding water, causing distribution of force to be unknown. Finally, why did the ACF react to the small strain witnessed in cycle 4, but not to the highest strain witnessed, cycle 3? This emphasizes that the ACF is calculated from the de-trended noise signal alone, $\epsilon_n(t)$ (Equation 3). A larger strain exerted on the wall should not lead to an increased probability of early detection of ice formation. However, considering the four successful indications, cycle 4 had the smallest measured strain and the most difficult to detect trend in the ACF. Therefore, perhaps the magnitude of the ACF indicator trend is dependent on the component strain, $\epsilon_0(t)$, but the probability of prediction is dependent on only the dynamical behavior witnessed in the noise, $\epsilon_n(t)$. This means to acquire a successful prediction that is easily detected, both dependencies are required to be met.

3 CONCLUSION

The work in this paper set out to determine if water-ice transitions could be predicted using tipping point analysis. The potential applications for this method include the prevention of freeze-thaw damage in concrete and ice build-up on wind turbine blades. Of the presented experimental data which included seven freezing cycles within an open container, four cycles provided successful predictions around 5-10 minutes prior to freezing point. The other three cycles showed no false positives, since the autocorrelation function indicator did not rise, demonstrating the potential of this method to be applied in a real world application to alert of an imminent ice formation.

The choice of an open top container in an attempt to closely imitate some real world applications caused difficulty in modelling the system and exhibited random behavior during formation. For example, the strain did not correlate with mass due to the fact the location of ice formation is unknown and only one wall was instrumented. Perhaps instrumenting more walls would improve probability at the cost of more sensors. Nevertheless, promising results were acquired from the degenerate fingerprinting, as even strains in the magnitude of $13\mu\epsilon$ presented alerts. In future work a closed container will be used, although less relatable to the real world applications discussed, it will remove any dependency on component strain, $\epsilon_0(t)$, as this will be greater and less variable each cycle. With no air to displace, the force distribution should be equal throughout the container meaning one sensor should be sufficient. A more thorough model of strain relation

to mass would also be possible. Further methods of tipping point analysis will be explored to determine the most effective for this application.

4   REFERENCES

Bai, M. He, R. Ma, and D. Huang, "Structural condition monitoring of wind turbine foundations," 2016. ICE proceedings.

Cattin and U. Heikkila, "Evaluation of ice detection systems for wind turbines," 2015. Meteotest final report.

Chan, L. Yu, H. Y. Tam, Y. Q. Ni, S. Y. Liu, W. H. Chung, and L. K. Cheng, "Fiber Bragg grating sensors for structural health monitoring of Tsing Ma bridge: Background and experimental observation," Engineering Structures 28(5), pp. 648–659, 2006.

Dakos, S. Carpenter, W. Brock, A. Ellison, V. Guttal, A. Ives, S. Kefi, V. Livina, D. Seekell, E. van Nes, M. Scheffer, "Methods for Detecting Early Warnings of Critical Transitions in Time Series Illustrated Using Simulated Ecological Data", PLOS ONE, July 2012.

Gholaminejad and R. Hosseini, "A study of water supercooling," 2013. Journal of Electronics Cooling and Thermal Control.

Harrison, J. D. Dewar, B. V. Brown, "Freeze-thaw resisting concrete – its achievement in the UK", CIRIA C559, London 2001.

Hill and G. Meltz, "Fiber Bragg grating technology fundamentals and overview," 1997. Journal of Lightwave Technology, Vol. 15, No. 8.

Inaudi and B. Glisic, "Distributed fiber optic strain and temperature sensing for structural health monitoring," 2006.

Kashyap, "Fibre Bragg gratings," 2010. Second Edition, ISBN: 978-0-12-372579.

Ko, Y. Q. Ni, "Structural Health Monitoring and Intelligent Vibration Control of Cable-Supported Bridges: Research and Application, KSCE Journal of Civil Engineering, vol. 7, pp. 701-716, November 2003.

Li, "Durability design of concrete structures – Phenomena, Modeling, and Practice", First edition John Wiley & Sons, Singapore Pte. Ltd., ISBN: 9781118910092, pp. 56-78, 2016.

Lima, R. Vicente, R. Nogueira, I. Abe, P. Andre, C. Fernandes, H. Rodrigues, H. Varum, and H. Kalinowski, "Structural health monitoring of the church of Santa casa de Misericordia of Aveiro using FBG sensors," 2008. IEEE Sensors Journal.

Livina, E. Barton, A. Forbes, "Tipping point analysis of the NPL footbridge", Journal of Civil Structural Health Monitoring, 2013.

Livina, T.M. Lenton, "A modified method for detecting incipient bifurcations in a dynamical system", Geophysical research letters, vol. 34, 2007.

Nicolas, R. Sullivan, and w. Richards, "Large scale applications using FBG sensors: Determination of in-flight loads and shape of a composite aircraft wing," 2016. Aerospace 2016, 3, 16.

Niewczas and G. Fusiek, "Induction Heated Assisted Optical Fibre Bonding and Sealing Technique," 21st International Conference on Optical Fiber Sensors 7753, pp. 77536H–77536H–4, 2011.

Orr, P. Niewczas, A. Dysko, and C. Booth, "FBG-based fibre-optic current sensors for power systems protection: Laboratory evaluation," 2009. The 44th International Universities' Power Engineering Conference.

Perry, V. Livina, and P. Niewczas, "Tipping point analysis of cracking in reinforced concrete", 2015. Smart Materials and Structures, vol. 25, No. 1.

Rao, "In-fibre Bragg grating sensors", review article, Measurement Science and Technology 8, pp. 355-375, PII: S0957-0233(97)72999-0, November 1996.

Scottish Government, "Energy statistics for Scotland," 2016.

Sen, K. Bhuwanesh, K. Ashutosh, Z. Engineer, S. Hedge, P.K. Sen, R. Lal, "Micro-scale multi-effect distillation system for low steam inputs", 5th BSME International Conference on Thermal Engineering, v. 56, pp. 63-67, 2013.

Stott, J O.M. Karlsson "Visualization of intracellular ice formation using high-speed video cryomicroscopy", 2008, Cryobiology 58, 2009, pp. 84-95.